Structural Investigation of the Thermal Decomposition of Ammonium Heptamolybdate by in situ XAFS and XRD

Julia Wienold,[a] Rolf E. Jentoft,[a] and Thorsten Ressler*[a]

Keywords: X-ray absorption spectroscopy / X-ray diffraction / Molybdenum / Polyoxometalates

The decomposition of ammonium heptamolybdate (AHM, $(NH_4)_6Mo_7O_{24}\times4H_2O$) was studied in situ by X-ray diffraction and X-ray absorption spectroscopy, as well as by thermal analysis (TG/DTA). Decomposition conditions such as reactant atmospheres, (20% oxygen, 5% propene, 5% hydrogen, pure helium, and static air), heating rates, and gas flow rates were varied to investigate their influence on the decomposition process. The results obtained show that the reaction pathway is affected by the partial pressures of the gas-phase decomposition products. The partial pressures of the decomposition products, water and ammonia, at a given temperature, is influenced mainly by the reactant gas flow rate and the heating rate. Lowering the partial pressures of ammonia and water inhibits the crystallization of the intermediate ammonium tetramolybdate (ATM), and promotes the formation of the intermediate hexagonal MoO_3. The decomposition pathway under low gas phase product partial pressure is: (i) AHM; (ii) (ca. 335 K) X-ray amorphous phase; (iii) (ca. 520 K) hexagonal MoO_3; (iv) (ca. 650 K) the products, which depend on the reactant atmosphere, are mixtures of highly disordered Mo_4O_{11}, and/or α-MoO_3. Under different conditions the decomposition pathway is: (i) AHM; (ii) (ca. 350 K) X-ray amorphous phase; (iii) (ca. 470 K) ATM; (iv) (ca. 570 K) hexagonal MoO_3 + α-MoO_3; (ca. 650 K) α-MoO_3. Under a hydrogen containing atmosphere, a peculiar decomposition pathway is observed: an intermediate MoO_3 with an unusual texture is formed prior to the reduction to MoO_2 and the consecutive formation of orthorhombic Mo_4O_{11}.

Introduction

Numerous authors have investigated the thermal decomposition of ammonium heptamolybdate tetrahydrate [$(NH_4)_6Mo_7O_{24}\times4H_2O$, AHM] using several techniques.[1−24] The decomposition pathway of AHM has been the subject of most studies.[2−13,19,23,24] Thermogravimetric analysis [TGA] and/or differential thermal analysis [DTA],[2−12,19,24] infrared spectroscopy [IR],[6,9,12] and X-ray diffraction [XRD][3−7,9,10] have been used to identify the intermediates and final products. Other studies have compared the decomposition of AHM with that of compounds with similar composition.[8,18−21] The decomposition of AHM was also investigated with respect to the effect of varying decomposition conditions. The influence of dopants, such as vanadium,[14] cobalt,[15] and alkali metal ions,[16] the influence of supports,[17,19,22] and the influence of reactant atmosphere has also been investigated.[1,23] In most studies, flowing or static air was used, the exceptions being the studies by Yong (1990)[13], Thomazeau (2000),[22] and the thermo-Raman study by Murugan (2001),[23] which were carried out under H_2, Ar, and N_2 and O_2, respectively. The TG study by Hegedüs (1957),[1] was carried out under a variety of different atmospheres.

In Table 1, the results of several representative studies are summarized. For comparison, the total amounts of molybdenum and oxygen, reported in the formulas from the literature, were normalized to five molybdenum atoms for the first step (this phase is mostly reported as pentamolybdate), and eight molybdenum atoms for the second step (this phase is mostly reported as octamolybdate). Normalization was done without changing the stoichiometry and is valid since the reported stoichiometric formulae were all based on chemical analyses and not on structural analyses. Although four decomposition stages can be distinguished, as indicated in Table 1, not all the authors observed all stages, and the temperatures of the decomposition steps vary. The first step takes place at temperatures of about 370 K (335−400 K), affording $(NH_4)_4Mo_5O_{17}$ as an intermediate. At about 470 K (430−510 K), the second decomposition step takes place, and the intermediate formed is reported to be $(NH_4)_4Mo_8O_{26}$, with the exception of study 7. In studies 4, 5, and 6, the formation of hexagonal intermediates ($MoO_3 \times xH_2O \times yNH_3$) at about 520 K (510−545 K) is reported as the third step. The final step in all the studies is the formation of α-MoO_3 (orthorhombic), with the corresponding temperatures varying from 540 K to 630 K. In two studies, 4 and 6, this step is preceded by the formation of a hydrous MoO_3 species.

[a] Department of Inorganic Chemistry, Fritz-Haber-Institut der MPG
Faradayweg 4−6, 14195 Berlin, Germany
Fax: (internat.) + 49-30/8413-4405
E-mail: Ressler@FHI-Berlin.MPG.de

Table 1. Results of the study of AHM decomposition from selected publications

No.	Publication	Conditions; method			
		Decomposition scheme			
1	Ma et al., 1963	Static air; 7 K/min; TG/DTA, ex situ XRD characterization			
		400 K → $(NH_4)_4Mo_5O_{17;}$	510 K → $(NH_4)_4Mo_8O_{26}$		630 K → α-MoO_3
2	Schwing-Weill, 1967	No information on atmosphere and flow rate; 0.25 K/min; TG, ex situ XRD characterization and chemical analysis			
		370 K → $(NH_4)_4Mo_5O_{18;}$	460 K → $(NH_4)_4Mo_8O_{26}$		575 K → α-MoO_3
3	Louisy et al., 1970	static air; 0.25 K/min / TG/DTA, ex situ XRD characterization			
		350 K → $(NH_4)_4Mo_5O_{17}$	430 K → $(NH_4)_4Mo_8O_{26}$	525 K → dodecamolybdate	540 K → α-MoO_3
4	Kiss et al., 1970	Air; 277 ml/min; 5 and 10 K/ min; TG/DTA, in situ IR analysis of gaseous products, ex situ XRD and IR characterization			
		370 K → $(NH_4)_4$*$Mo_5O_{17;}$	(430 K → pseudo octamolybdate) 480 K → $(NH_4)_4Mo_8O_{26}$	530 K→$(NH_4)_2O$*$Mo_{14}O_{42}$(hex.) 545 K→$(NH_4)_2O$*$Mo_{22}O_{66}$(hex.)	550 K → MoO_3*× H_2O 570 K → α-MoO_3
5	Isa et al., 1981	static air 3 K/min; TG/DTA, in situ XRD analysis			
		335 K → decomposition starts	445 K → $(NH_4)_4Mo_8O_{26}$ + hex. MoO_3	525 K→ hex. MoO_3	630 K → α-MoO_3
6	Hanafi et al., 1980	No information on atmosphere and flow rate; 1.25 K/min; TG, ex situ XRD and IR characterization			
		370 K → $(NH_4)_4Mo_5O_{17;}$	480 K °C → $(NH_4)_4Mo_8O_{26}$	510 K→$(NH_4)_2O$*$Mo_{12}O_{36}$(hex.) 530 K→$(NH_4)_2O$*$Mo_{22}O_{66}$(hex.)	550 K → MoO_3*× H_2O 580 K → α-MoO_3
7	Said et al., 1994	Dry air; 40 ml/min; 10 K min; TG/DTA, ex situ XRD and IR characterization			
		395 K → $(NH_4)_{2.86}Mo_5O_{16,43}$*1.43$H_2O$	490 K → $(NH_4)_{2.28}Mo_8O_{25,14}$*2.28$H_2O$		575 K → α-MoO_3

In study 5, all the phases formed during the decomposition are identified in situ. This is the only study in which this is observed. In all the other studies, with the exception of study 6 where at least some intermediates are identified in situ, the characterization and identification of the intermediates and products were performed ex situ, and are based on chemical and XRD powder pattern analyses. The considerable variation in the reported decomposition step temperatures may be due to experimental conditions, i.e. different heating rates. The reasons for the differences in the observed phases and the wide temperature range for the formation of the final phase are not obvious. The results of study 5 are unique in that the first decomposition step is not observed at all, and after the second step at 445 K, two phases were reported, namely $(NH_4)_4Mo_8O_{26}$ and hexagonal MoO_3. In summary, although the decomposition process has already been studied to some extent, no description of the sequence of events that can explain the spread in materials and conditions of this key reaction in the production of molybdate heterogeneous catalysts exists.

An overview of the molybdenum-oxygen polyhedra found in the structures of the reported intermediates and products is presented in Figure 1. The structure of AHM is composed of monomers of seven distorted, edge-sharing, molybdenum-oxygen octahedra (Figure 1, A) [ICSD 4153]. The intermediate formed in the first step has been identified as $(NH_4)_4Mo_5O_{17}$, ammonium pentamolybdate, in several studies. Powder lines calculated from single crystal data of $(NH_4)_8Mo_{10}O_{34}$ [ICSD 67325] match the powder lines reported for this material [ICDD 21−971 and 26−77], and hence this intermediate can be identified as ammonium decamolybdate. This structure is composed of monomers of eight distorted, edge-sharing, molybdenum-oxygen octahedra and two distorted molybdenum-oxygen tetrahedra, which are linked to the cluster through bridging oxygen atoms. The resulting polyhedron is shown in Figure 1, B. The second intermediate, with the stoichiometry $(NH_4)_4Mo_8O_{26}$, can be identified as ammonium tetramolybdate, by comparing the literature powder lines [ICDD 18−117] with the powder diffraction data calculated from single crystal data of $(NH_4)_2Mo_4O_{13}$ [ICSD 68562]. In this structure, the distorted, edge-sharing, molybdenum-oxygen octahedra form one-dimensional oligomers, i.e. chains, as seen in Figure 1, C. The last intermediate is reported to be hexagonal. In studies 4 and 6, two phases with different stoichiometry, occurring successively and at nearly the same temperature (530/545 K), are reported. The powder patterns given for these phases are very similar and can be simulated with one single crystal data set with slightly varied lattice constants. The corresponding phase is $(NH_3)(MoO_3)_3$ [ICSD 62163], which can be understood as a hexagonal MoO_3 with NH_3 intercalated in the lattice. This phase is built from a three-dimensional network of distorted, edge and corner-sharing, molybdenum-oxygen octahedra that form six-fold channels in the structure, see Figure 1 (see D). The structure of the final product, α-MoO_3 (orthorhombic), is shown in Figure 1 (see E) [ICSD 35076], and is built from planes which are made from edge- and corner-sharing, distorted molybdenum-oxygen octahedra. A row of corner sharing, distorted molybdenum-oxygen octahedra, as indicated in Figure 1, constitute the structural unit in both hexagonal and α-MoO_3.

Our particular interest in the decomposition of AHM is because of its use as a precursor in the production of mol-

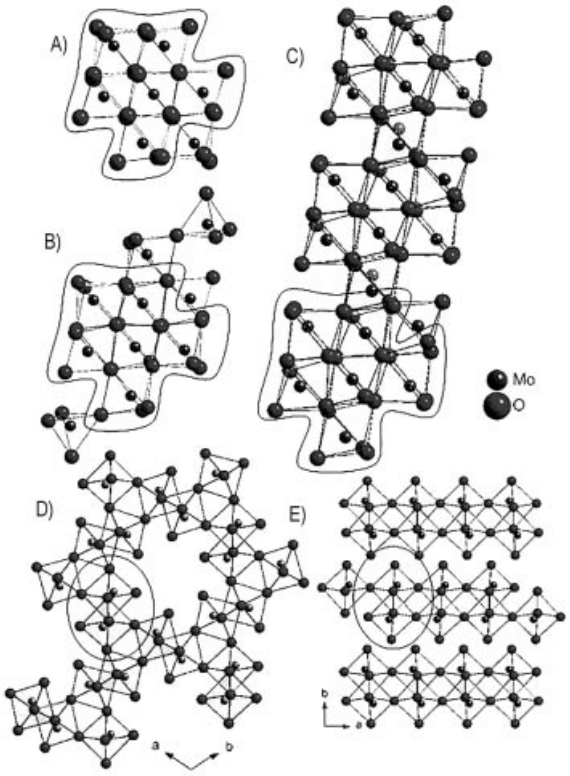

Figure 1. Schematic structural representation of potential intermediates in the decomposition of ammonium heptamolybdate: A, monomer of ammonium heptamolybdate; B, monomer of ammonium decamolybdate, C, sequence of the one-dimensional oligomer of ammonium tetramolybdate; D, hexagonal MoO_3 projected along the *c* axis; E, α-MoO_3 projected along the *c* axis. Only the molybdenum and oxygen atoms of the structures are shown. Ammonia and water are omitted. The structural units encircled in the monomers A and B and in the oligomer C are similar in all three phases. The structural units in hexagonal MoO_3 and α-MoO_3, encircled, indicate the rows of edge-shared octahedra, which are the same in the two structures

ybdenum trioxide (MoO_3) and partially reduced molybdenum oxide (MoO_{3-x}) catalysts. These oxides are suitable model systems[25] for the more complex mixed-oxide systems (molybdenum oxide with different additional components, for example Bi, W, V, Cu), which are used extensively as partial oxidation catalysts for light alkenes.[26] The catalytic activity of these materials depends on their properties,[27] i.e. their real structure (number and type of defects), their composition, and their particle sizes; which, in turn, will depend on the treatment of the precursor. Therefore, in order to learn how to control the textural and chemical properties of the resulting binary oxide, studies on the influence of different treatment parameters on the decomposition process, such as the composition of the gas phase or the heating rate, are required, together with a detailed analysis of the short- and long-range structure evolution.

In this work the decomposition of AHM is studied using in situ XRD and in situ X-ray absorption spectroscopy (XAS). The use of these two complementary methods allows us to follow the evolution of the short- and long-range structures of the phases formed. XRD is used to identify the phases and to reveal their crystallinity on a long-range order scale. The information gathered by XRD is used as a starting point for the analysis of the local structure by XAS. In addition, amorphous phases, which cannot be characterized by XRD, can be analyzed by XAS. The decomposition products in the gas phase are simultaneously analyzed by mass spectrometry. Additionally, the onset temperatures for the decomposition steps are obtained by TG/DTA coupled with evolved gas analysis (EGA) by mass spectrometry. Further, the influence of different atmospheres, such as pure helium, helium and oxygen, hydrogen, or propene, on the formation of intermediates and products is examined. In addition, the influence of the heating rate and the gas phase flow rate on the decomposition process is also investigated. The atmospheres are chosen to have oxidative, reductive, inert, and catalytically relevant reaction environments.

Results

Characterization of Ammonium Heptamolybdate

In Figure 2, the experimental diffraction pattern of ammonium heptamolybdate [$(NH_4)_6Mo_7O_{24}\times4H_2O$, AHM] in the range from 7 to 60° 2θ is shown, together with both the XRD powder pattern simulation employing single crystal data [ICSD 4153] (a = 8.393(1), b = 36.170(4), c = 10.472(1) Å, β = 116.0(0)°] and the difference between the experimental and simulated patterns. The refinement of the lattice parameters was performed with the software PowderCell 2.3. For the peak profile, the Pseudo-Voigt2 function was used and the full width at half maximum (FWHM) was taken as FWHM = $f(U,V,W)$, where only W was fitted and U = V = 0. The R_p value of the fit was 13.73. The resulting lattice constants are: a = 8.395(7), b = 36.204(3), c = 10.4765 Å, β = 115.884°. The good agreement between the experimental data and the single crystal data, the relatively small R_p value, and the fact that all the peaks in the experimental pattern of AHM were accounted for, indicate that the sample is pure and that the stoichiometry according to the structural formula is valid. The latter is also confirmed by the good agreement between the calculated and the measured weight loss for the decomposition of AHM in O_2/He with α-MoO_3 as the final product. In Figure 3, the IR absorption spectrum of AHM is shown. It is very similar to those previously reported for AHM and related compounds.[9,23,39,40] An assignment of the absorption bands is given in Table 2. For H_2O and NH_4^+, hydrogen bridging to the terminal oxygen of the Mo−O octahedra can be assumed from the structural data of AHM, whereas $O_{H2O}-O_{Molybdenum}$ = 2.72 Å and $N_{NH_4^+}-O_{Molybdenum}$ = 2.86 Å (stretching modes of H_2O at approximately 3400 cm^{-1} and of NH_4^+ at approximately 3100 cm^{-1}). The bending mode at 1640 cm^{-1} for H_2O refers to the free H_2O molecule. The bands below 1000 cm^{-1} are all assigned to the Mo−O modes, with the exception of the H_2O vibration mode at 636 cm^{-1}.

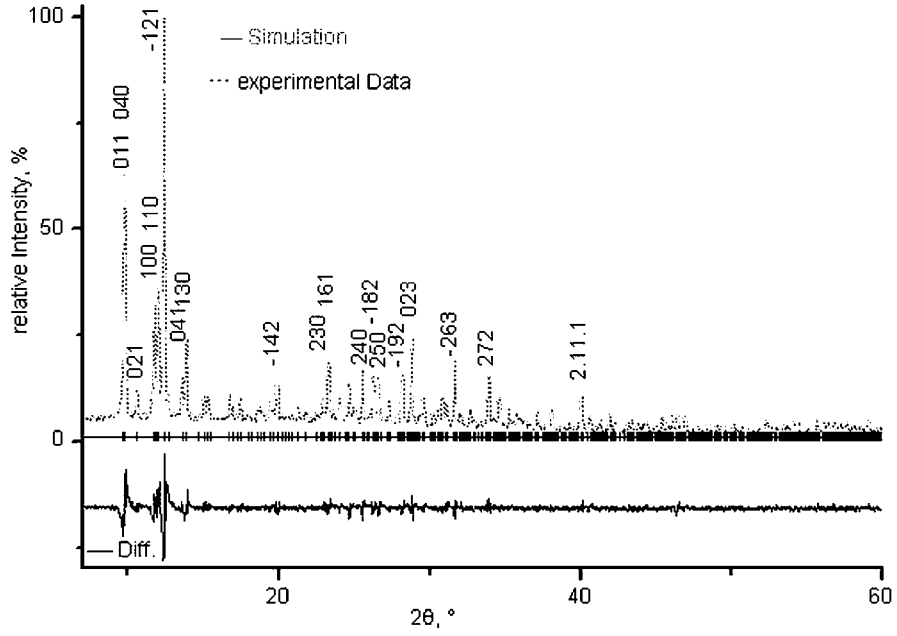

Figure 2. X-ray pattern of AHM (Aldrich), together with the fit of the theoretical data and the difference curve. Only the indices of peaks with $I_{rel.} > 5\%$ are given for clarity

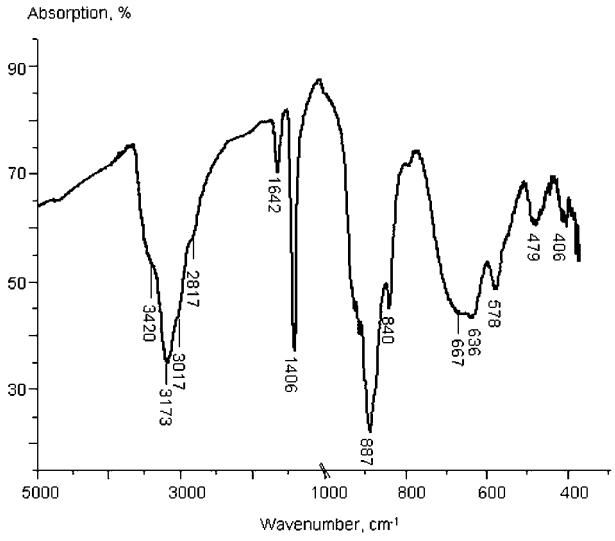

Figure 3. IR spectra of AHM (Aldrich). The *x*-axis is divided into two sections with different increments for clarity. Wavenumbers of distinct absorption bands are given. An assignment of the bands can be found in Table 2

Table 2. Vibrational spectrum for $(NH_4)_6Mo_7O_{24}\times4H_2O$ (in cm^{-1})

IR	Assignment
3420 (sh)[a]	$\nu(H_2O)$
3173 (vs)	$\nu(NH_4^+)$
3017 (sh)	$\nu(NH_4^+)$
2817 (sh)	
1642 (m)	$\delta(H_2O)$
1406 (vs)	$\delta(NH_4^+)$
925 (sh)	ν(Mo−O)
915 (sh)	
887 (vs)	ν(Mo−O)
875 (sh)	
840 (m)	
792 (vw)	
667 (m)	ν(Mo−O)
636 (m)	Lib. H_2O
578 (m)	ν(Mo−O)
479 (m)	
406 (m)	

[a] vs: very strong, s: strong, m: medium, w: weak, vw: very weak, sh: shoulder

TG/DTA

Figure 4 shows the progression of the TG curve, together with the DTA signal and the MS signals for $m/z = 18$ (assigned to H_2O) and $m/z = 15$ (assigned to NH), during the decomposition of AHM in 20% oxygen with a heating rate of 5 K/min. Four decomposition steps at 320, 460, 530, and 635 K, characterize the evolution of the weight loss, with a continuous weight loss between the first and the third decomposition steps. The change in the slope of the TG curve, corresponding to the second decomposition step at 460 K, is small and can only be observed in the first derivative of the curve. The weight loss after the third decomposition step at 530 K amounts to 17.22%, and after the fourth step at 635 K, to 18.61%. The latter value is in agreement with the calculated weight loss of 18.48%, if α-MoO_3 is assumed to be the decomposition product of the starting material $(NH_4)_6Mo_7O_{24}\times4H_2O$. During the first decomposition step, two endothermic DTA signals can be distinguished. The third decomposition step also shows endothermic character, while the second and fourth steps are exothermic. With the exception of the first step, which

begins with the evolution of water only, all steps are accompanied by the evolution of water and ammonia. The TG curve and the corresponding DTA signals for the decomposition of AHM in pure helium are almost identical to those obtained for the decomposition under a 20% O_2 atmosphere at the same heating rate of 5 K/min. The only difference is the slightly greater total weight loss of 18.95% after the last decomposition step at 635 K, instead of 18.61%.

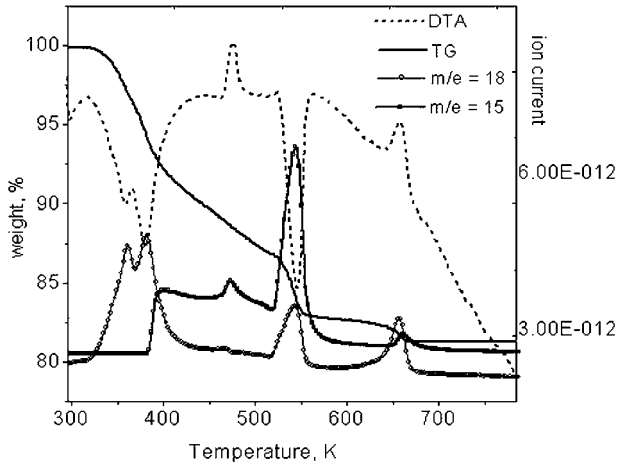

Figure 4. Evolution of the weight loss during decomposition of ground AHM in 20% oxygen in helium, together with MS signals for H_2O and NH_2^- and DTA signal (no axis inscription for the DTA signal). Heating rate: 5 K/min, flow rate: 100 mL/min

The influence of the different heating rates on the TG curve is shown in Figure 5. Lowering the heating rate from 5 K/min to 0.5 K/min does not affect the overall shape of the TG curve, however, the decomposition steps occur at lower temperatures and the weight loss prior to the third decomposition step increases. When the heating rate is increased from 5 K/min to 15 K/min, the overall shape of the TG curve changes. At this heating rate (15 K/min), the second decomposition step is accompanied by a visible change in the slope of the TG curve, resulting in a discernible stage. The total weight loss before the third decomposition step is less at the higher heating rate, and after the third decomposition step the weight loss increases from 17.22% to 18.03%. The total weight loss after the last step remains unchanged. All the decomposition steps take place at higher temperatures, except for the last step.

The influence of the heating rate and the gas flow on the TG curve is shown in Figure 6. A similar effect is observed on changing from a flowing to a static gas phase, as is seen on increasing the heating rate, i.e. lower weight loss at a given temperature and more distinct steps. A combination of accelerating the heating rate and a static gas phase results in a TG with four distinct decomposition steps, each resulting in a distinct stage. The corresponding weight loss for the steps is 6.63, 11.21, 18.03, and 18.6%. The weight

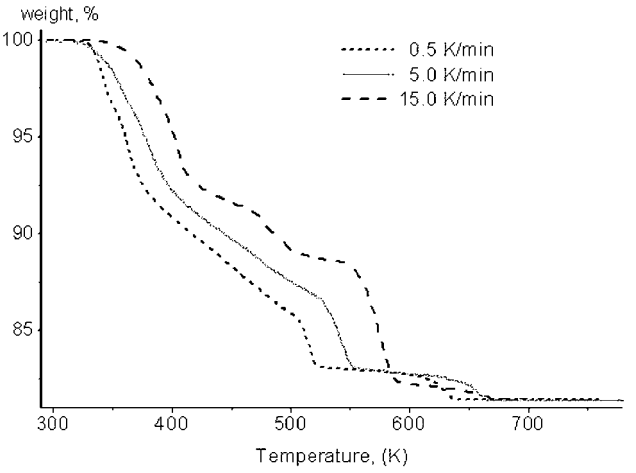

Figure 5. Comparison of the weight loss during decomposition of AHM in 20% oxygen in helium, flow rate 50 mL/min, with heating rates of 0.5, 5, and 15 K/min

loss for the first step is in excellent agreement with the calculated weight loss for the decomposition of AHM into ammonium decamolybdate (6.68%), and the second step corresponds to the formation of ammonium tetramolybdate with a weight loss of 11.09%.

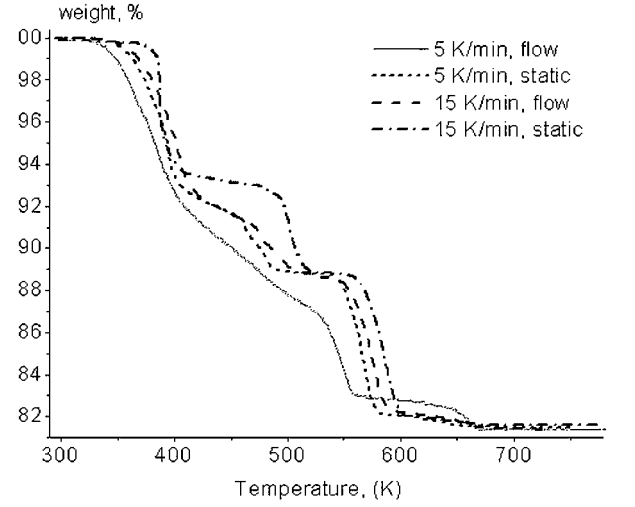

Figure 6. Comparison of the weight loss during decomposition of AHM in 20% oxygen in helium, flow rate 50 mL/min, with heating rates 5 and 15 K/min, and during decomposition of AHM in static air with heating rates of 5 and 15 K/min

The DTA signals in Figure 7 indicate that the exothermic character of the second decomposition step in Figure 4 is changed to an endothermic signal as the decomposition step becomes more pronounced due to the more rapid heating and static conditions as described above. Similarly, the exothermic signal of the last decomposition step becomes less distinct or is missing.

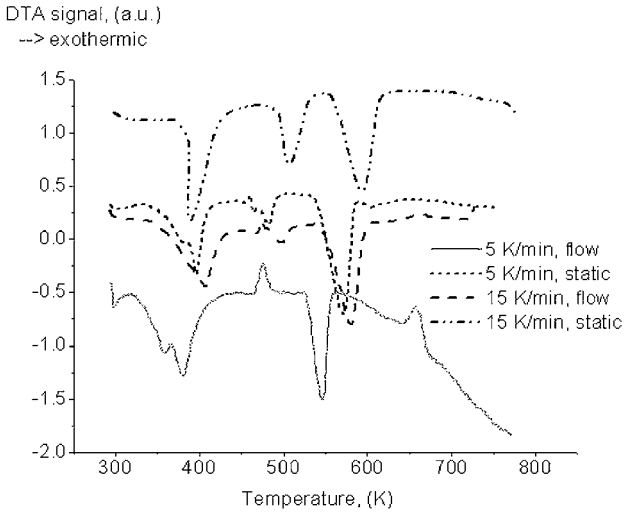

Figure 7. Comparison of the DTA signals, which belong to the TG curves shown in Figure 6. The DTA signals of the decomposition of AHM, 50 mL/min, 20% oxygen in helium, 0.5 K/min, are not shown, due to their weakness

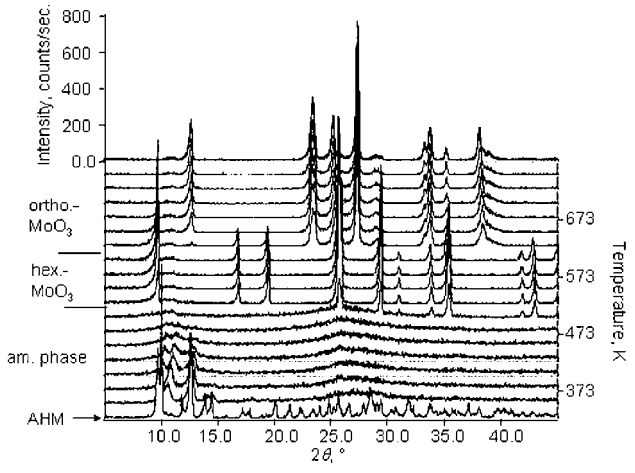

Figure 8. Evolution of the X-ray diffraction pattern during decomposition of AHM in 20% oxygen in helium. room temp. 770 K; effective heating rate: 0.1 K/min, Temperature held every 25 K for measurement; flow rate: 100 mL/min. The phases formed are indicated in the figure

In situ XRD and in situ XAS

Decomposition in 20% Oxygen

Figure 8 shows the evolution of the diffraction patterns during the decomposition of ground AHM in 20% oxygen with an effective heating rate of 0.1 K/min. Three distinct steps are visible in the diffraction patterns. In the first pattern at 320 K, changes from the expected pattern of AHM at room temperature are already observed, indicating that the decomposition has started. The patterns up to 420 K show a rapid decrease in crystallinity, and at 420 K show an X-ray amorphous phase. At 520 K, the formation of a new phase is observed which is identified as hexagonal $[H(_2O/NH_3)](MoO_3)_3$ [ICSD 62163], see Figure 1 (see D, denoted as hexagonal MoO_3 in the following). The splitting of the diffraction peak at approximately 25.7° 2θ with increasing temperature, can be explained by an expansion along the *a* and *b* axes. At 600 K, the hexagonal MoO_3 is transformed into α-MoO_3 [ICSD 35076]. Refinement of the lattice parameter of α-MoO_3 at 770 K affords a = 3.98(5) Å [3.96 Å], b = 14.222(3) Å [13.855 Å], c = 3.69(1) Å [3.69 Å] (the values in brackets are the initial values from the single crystal data [ICSD 35076] at room temperature). The variation of the lattice parameters indicates an anisotropic thermal expansion, which has also been reported by Kierkegard (1964).[33] The XRD investigations in 20% oxygen were performed with both, long and short ranges of 2θ in the XRD measurements, i.e. with effective heating rates of 0.1 K/min and 1 K/min. No differences are observed in the phases formed and the corresponding temperatures with the different effective heating rates.

Figure 9 (see A) shows the in situ XRD patterns obtained during the decomposition of AHM in 20% oxygen and with an effective heating rate of 1 K/min (short range of 2θ). The evolution of the radial-distribution-function {[FT(χ(*k*))],

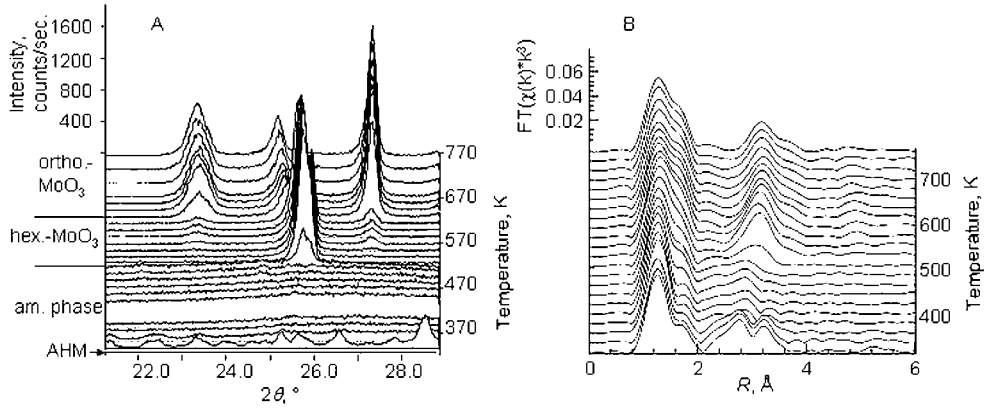

Figure 9. **A**: Evolution of the X-ray diffraction pattern during decomposition of AHM in 20% oxygen in helium. room temp. 770 K; effective heating rate: 1 K/min, Temperature held every 25 K for measurement; flow rate: 100 mL/min. **B**: Evolution of the radial distribution function (RDF) during decomposition of AHM in 20% oxygen in helium. Heating rate: 5 K/min, flow rate: 40 mL/min. The phases formed are indicated in the figure

RDF} from the corresponding in situ XAS experiment is presented in Figure 9 (see B). At the start of the decomposition process, the RDF corresponds to that of AHM. At about 345 K, the RDF exhibits a pronounced decrease in amplitude of the shells above 2 Å, indicating a loss of structural order. A comparison of the RDFs obtained between 450 K and 550 K and the RDF of crystalline ATM (the experimental RDF of ATM at 500 K is displayed in Figure 10) shows an agreement in the nodes and a comparable shape of the curve, and despite some small differences in the amplitudes, indicates a similar short-range order. At 520 K, a distinct change in the RDF occurs, corresponding to the phase change observed from the XRD data. However, in contrast to the XRD data, the RDF at about 600 K does not indicate the formation of a new phase. Despite the lack of changes in the RDF at 600 K, the simultaneously obtained MS data reveal the evolution of water and ammonia at 600 K, hence indicating a decomposition step. Although the hexagonal MoO_3 and the α-MoO_3 possess different long-range structures (see Figure 1, D and E), the pair distribution functions of the two phases within 6 Å are very similar, as is expected for phases which share the same structural features, as indicated in Figure 1. An overview of the bond lengths and coordination numbers of the two phases is given in Table 3. XAFS refinements on the RDFs between 520 K and 770 K, employing paths calculated with the FEFF7 code for either one of the two phases, result in similar distances (±0.05 Å). In Figure 11, the experimental RDF at 670 K is shown, together with a refinement using phases and amplitudes calculated for α-MoO_3.

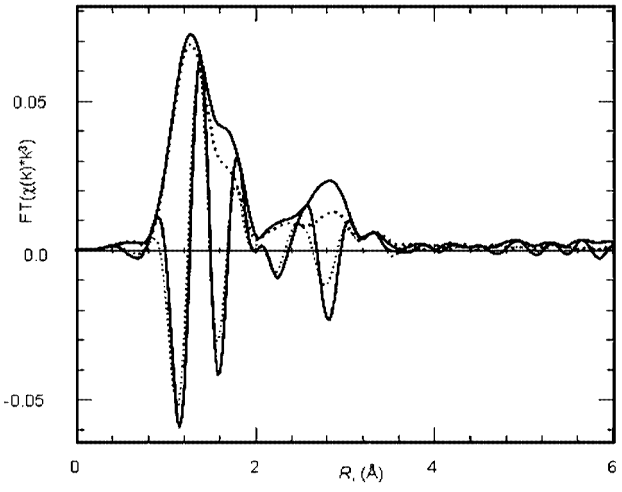

Figure 10. Comparison of the radial distribution function measured at 500 K during the decomposition in 20% oxygen (—) and the radial distribution function of ATM (· · · · ·)

Decomposition in Pure Helium

In Figure 12, A, diffraction patterns measured during the decomposition of AHM in pure helium with an effective heating rate of 1 K/min are presented. Figure 12, B shows the RDFs obtained from XAS measurements during the decomposition of AHM in pure helium. The evolution of the diffraction patterns for temperatures up to 600 K is similar to that observed for the decomposition of AHM in 20% oxygen. At temperatures above 600 K, the pattern of α-MoO_3 begins to show broad shoulders that can be identified as poorly crystallized Mo_4O_{11} (both monoclinic and orthorhombic). Mo_4O_{11} crystallizes with increasing temperature, without a decrease in the absolute intensity of α-MoO_3. The ratio between the monoclinic and orthorhombic Mo_4O_{11} phases changes from about 1:1 to 3:1 during crystallization. At 620 K, the evolution of the RDF during the decomposition of AHM in pure helium with a heating rate of 5 K/min exhibits a phase change, in contrast to the decomposition of AHM in 20% oxygen. The RDF of the phase formed at 620 K remains unchanged on further heating, i.e. there is no change in the short-range order with increasing temperature, in contrast to the changes in the long-range order observed with XRD. The evolution of the edge-shift with temperature, corresponding to the evolution

Table 3. Comparison of the distances between the central molybdenum atom and the surrounding atoms and coordination numbers of α-MoO_3 and hexagonal MoO_3

α-MoO_3			Hexagonal MoO_3		
Mo−O	1	1.671	Mo−O	1	1.645
Mo−O	1	1.734	Mo−O	1	1.687
Mo−O	2	1.948	Mo−O	2	1.941
Mo−O	1	2.251	Mo−O	1	2.210
Mo−O	1	2.332	Mo−O	1	2.378
Mo−Mo	2	3.438	Mo−Mo	2	3.299
Mo−O	2	3.552	Mo−O	2	3.563
Mo−O	2	3.554	Mo−O	2	3.694
Mo−Mo	2	3.696	Mo−Mo	2	3.726
Mo−O	1	3.764	Mo−O	1	3.755
			Mo−O	2	3.866
Mo−Mo	2	3.963	Mo−Mo	2	4.034
Mo−O	2	4.002			

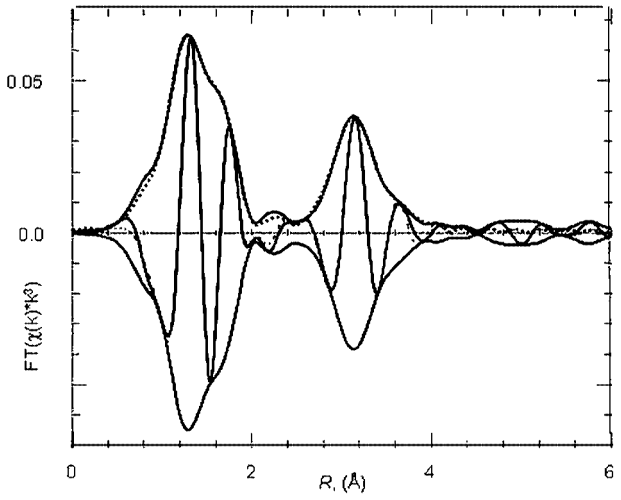

Figure 11. RDF of the decomposition in 20% oxygen in helium at 670 K (—) and the fit result of the simulation with single crystal data (· · · · ·). (*R*-value of the fit: 4.2)

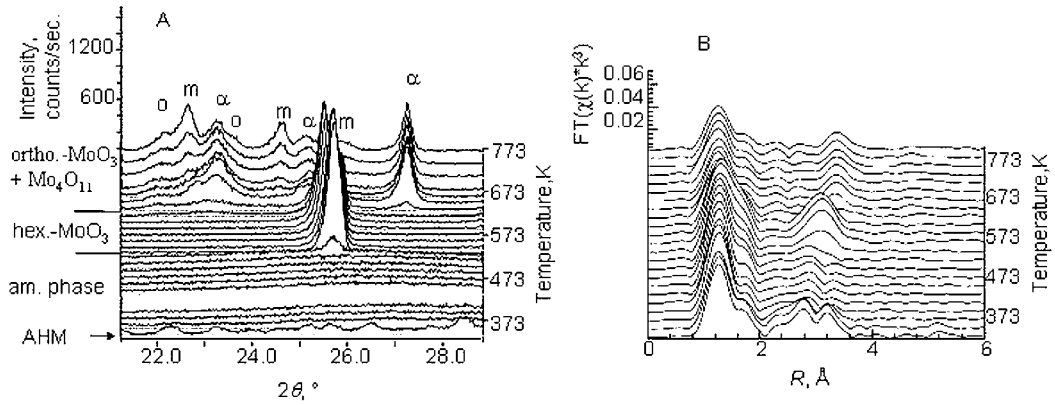

Figure 12. A: Evolution of the X-ray diffraction pattern during decomposition of AHM in helium. room temp. 770 K; temperature held every 25 K for measurement; effective heating rate: 1 K/min, flow rate: 100 mL/min. o: orthorhombic Mo_4O_{11}, m: monoclinic Mo_4O_{11}, α: orthorhombic MoO_3. B: Evolution of the RDF during decomposition of AHM in helium. Heating rate: 5 K/min, flow rate: 40 mL/min. The phases formed are indicated

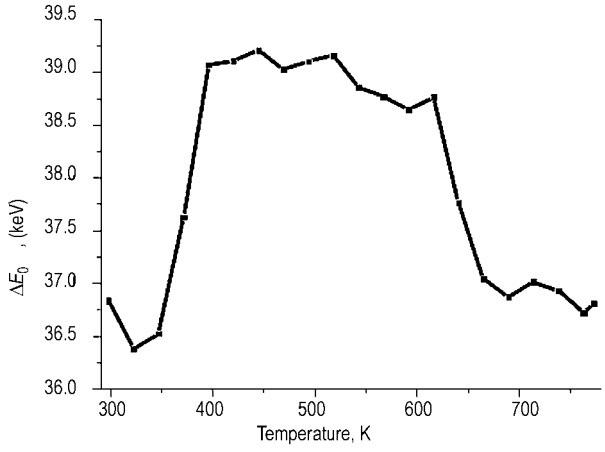

Figure 13. Evolution of the edge-shift with temperature from in situ XAS data of the decomposition of AHM in helium

of the radial distribution functions in Figure 12, B, is shown in Figure 13.

Decomposition in 5% Propene

The evolution of the diffraction patterns measured during the decomposition of AHM in 5% propene in helium with an effective heating rate of 1 K/min is shown in Figure 14, A. The corresponding RDFs are presented in Figure 14, B. For temperatures up to 600 K, the evolution of diffraction patterns is similar to that observed for the decomposition of AHM in pure helium or in 20% oxygen. At 620 K, poorly ordered orthorhombic and monoclinic Mo_4O_{11} is formed as intermediates. Subsequently, these phases are reduced to MoO_2, and at 700 K, the reduction to MoO_2 is complete. MoO_2 remains unchanged on further heating. In order to characterize the Mo_4O_{11} formed, this phase was isolated in situ, by stopping the flow of propene at the temperature of its formation, thus preventing further reduction to MoO_2. The evolution of the diffraction pat-

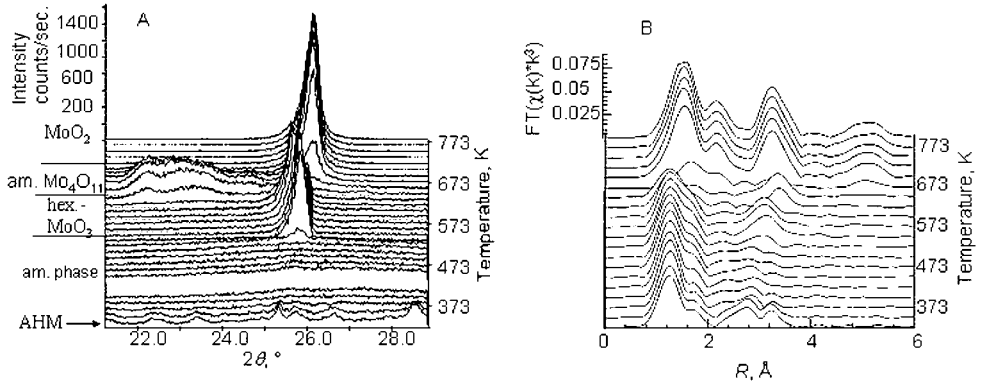

Figure 14. **A**: Evolution of the X-ray diffraction pattern during decomposition of AHM in 5% propene in helium. room temp. 770 K; temperature held every 25 K for measurement; effective heating rate: 1 K/min, flow rate: 100 mL/min. B. Evolution of the RDF during decomposition of AHM in 5% propene in helium. Heating rate: 5 K/min, flow rate: 40 mL/min. The phases formed are indicated

terns in the temperature range from 700 K to 770 K shows progressive crystallization of Mo_4O_{11}. A small amount of α-MoO_3 is also detected, and its absolute intensity remains constant with increasing temperature. The ratio between monoclinic and orthorhombic Mo_4O_{11} changes from about 1:2 to 1:1 during crystallization.

The evolution of the RDF during decomposition in 5% propene is similar to that during the decomposition in helium up to ca. 600 K. At 620 K, the RDF during the decomposition in 5% propene indicates a phase change. The phase formed is rapidly transformed into MoO_2, and can be identified at 645 K. The MoO_2 is identified by simulation of the RDF with an extended fine structure calculated from single crystal data.

Decomposition in Hydrogen

Figure 15, A shows the evolution of the diffraction patterns measured during the decomposition of AHM in 5% hydrogen with an effective heating rate of 1 K/min. Up to 520 K, the evolution of the diffraction patterns is similar to those described above. At 520 K, α-MoO_3 is obtained, in contrast to the decomposition processes in oxygen, helium, or propene where hexagonal MoO_3 is detected at 520 K. The α-MoO_3 formed possesses a strong preferred orientation which can be described as platelets with a (110) basal plane, according to the model of March.[34] This is different from the common (010) texture effects for α-MoO_3. The reduction of this phase to MoO_2 begins at 655 K, and at 745 K, the formation of Mo_4O_{11} is detected. Under these condition only the orthorhombic phase of Mo_4O_{11} is observed.

Evolution of the RDF of AHM during decomposition in 20% hydrogen is shown in Figure 15, B. The evolution of the RDF up to 620 K is similar to that in helium, and to that in 20% oxygen in helium. At about 600 K, the RDF of α-MoO_3 and/or hexagonal MoO_3 can be identified by comparison of the experimental RDF with a theoretical RDF of α-MoO_3. From 620 K to 770 K, the RDF changes continuously, corresponding to the formation of MoO_2.

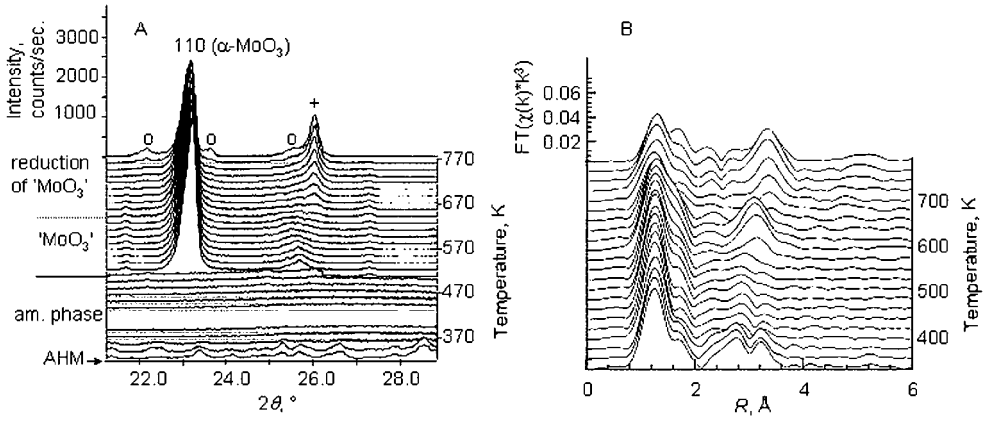

Figure 15. A: Evolution of the X-ray diffraction pattern during decomposition of AHM in 5% H_2 in helium. room temp. 770 K; temperature held every 25 K for measurement; effective heating rate: 1 K/min, flow rate: 100 mL/min. o: orthorhombic Mo_4O_{11}, +: MoO_2. B: Evolution of the RDF during decomposition of AHM in 20% H_2 in helium. Heating rate: 5 K/min, flow rate: 40 mL/min. The phases formed are indicated

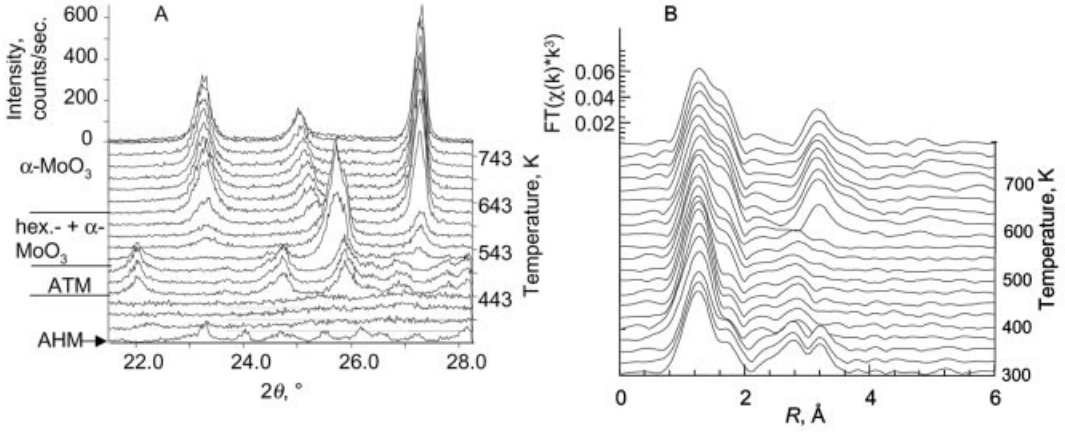

Figure 16. A: Evolution of the X-ray diffraction pattern during decomposition of AHM in static air. room temp. 770 K; temperature held every 25 K for measurement; effective heating rate: 1 K/min. B: Evolution of the RDF during decomposition of AHM in static air. Heating rate: 5 K/min, flow rate: 40 mL/min. The phases formed are indicated in the figure

Decomposition in Static Air

In Figure 16, the evolution of the diffraction patterns (1 K/min) and the RDFs measured during the decomposition of AHM in static air (5 K/min) are shown. Analysis of the XRD data shows that after the formation of an X-ray amorphous phase, ammonium tetramolybdate {ATM, $(NH_4)_2Mo_4O_{13}$, [ICSD 68562]} crystallizes at about 450 K. At 550 K, ATM decomposes into hexagonal MoO_3 and α-MoO_3. At 600 K, hexagonal MoO_3 transforms into α-MoO_3.

The evolution of the RDFs of AHM during decomposition in static air is similar to that during the decomposition in 20% O_2 (Figure 9, B). The formation of either hexagonal or α-MoO_3 can be seen at 640 K, instead of 620 K as in the decomposition in 20% O_2. During decomposition, the temperatures corresponding to the transformation of ATM to α-MoO_3/hexagonal MoO_3 in static air obtained from the XRD analysis are different from those obtained from the evolution of the RDFs (550 and 640 K, respectively). These differences may be attributed to a combination of the differences in the heating rates (1 or 5 K/min for XRD or XAS, respectively), and the differences in the reactor volume, which, under static conditions, may affect the gas phase composition.

Discussion

The experiments presented were performed to elucidate a reaction scheme for the decomposition of ammonium heptamolybdate, AHM, and to determine the effect of the gas phase composition, heating rate, and gas phase flow rate on the decomposition pathway. The emphasis herein was to obtain phase sequences from a phenomenological analysis of in situ experiments under controlled and comparable conditions. The results show that the decomposition scheme and the products formed are strongly influenced by the composition of the gas atmosphere in which the decomposition process takes place. Both the type of gas feed to the system, and the degree to which gas phase products are removed during the decomposition are important. These dependencies, hitherto not systematically recognized, and the knowledge of the sequence of phases formed during the various paths of decomposition explain the differences in the results which have been reported in the literature, and described in the introduction of this paper.

The TG/DTA experiments reveal that the pathway of the decomposition, i.e. the number of decomposition stages (Figures 4, 5, and 6) and the exothermicity or endothermicity of the step (DTA, Figure 7), depend on the heating rate and the gas flow rate. These observations suggest that all the reaction steps for the formation of α-MoO_3 from AHM are kinetically controlled. The extrinsic control variables, i.e. the processes at the gas-solid interface, including the transport of molecules and energy, are important for the reaction sequences. The intrinsic parameters, such as non-stoichiometry or morphology of the precursor, are not ruled out as additional control variables, however, these parameters were not investigated here.

The decomposition can be controlled, by the gas flow rate and the heating rate, to proceed through two phenomenologically different decomposition pathways: one with an extended region of continuous weight loss after the first decomposition step, denoted as Pathway 1; or alternatively through four distinct decomposition stages, denoted as Pathway 2 (Figures 4−6). Intermediate pathways in which the first and second decomposition stages are not pronounced can also be observed. Both pathways are characterized by DTA signals, and by the MS signals of water and ammonia, which indicate a decomposition process that occurs in four steps.

The heating rate and the gas flow rate affect the decomposition process in a similar manner, as indicated by the TG curves. The common parameter which influences the decomposition process is the partial pressure of the gas phase decomposition products, water and ammonia. The temperature at which decomposition occurs is dependent on the partial pressures of the gas phase products, which in turn is dependent on the heating rate and/or gas flow rate. The partial pressures of the gas phase products determine their availability for interaction with the solid. Decreasing the heating rate or increasing the gas flow rate reduces the partial pressure of ammonia and water and allows the decomposition to proceed at lower temperatures without the formation of distinct stages. Conversely, increasing the heating rate and/or decreasing the reactant gas flow rate increases the partial pressure of ammonia and water in the gas phase, stabilizes intermediate phases, and hence results in distinct stages. Under these conditions the decomposition progresses with distinct steps and stages. A similar correlation between the decomposition pathway and the interaction of the gas phase decomposition products with the base material has also been discussed by Maciejewski et al. (2000) for the decomposition of cobalt oxalate dihydrate.[35] They found that the primary gas- and solid-phase products reacted in secondary gas-solid and gas-gas reactions. Similarly, we suggest that the crystallization processes of the molecular structures of the intermediates after the first and second decomposition step, ammonium decamolybdate (possibly X-ray amorphous phase A), and ammonium tetramolybdate, may require water and/or ammonia as ligands. The crystallization of these intermediates results in the process of polycondensation (the formation of hexagonal MoO_3 and/or α-MoO_3) occurring at higher temperatures. The formation of hexagonal MoO_3 decreases with the formation of crystalline ATM, and thus appears to be induced by the low partial pressure of gaseous water and ammonia.

The kinetic reaction control discussed above would suggest that the effect of reactant gas composition on the decomposition pathway be studied at low heating rates, conditions under which product gases are purged and gas phase diffusion limitations are minimized. Such conditions allow analysis of the decomposition by structurally sensitive in situ XRD and in situ EXAFS experiments. Figure 5 indic-

ates that no qualitative changes are introduced into the sequence of events at low heating rates. Differences in the onset temperatures of the phase changes observed can be expected (≈ 20 K), because of the different heating rates.

From in situ XRD and XAS measurements, the sequence of phase transformations corresponding to the decomposition steps was elucidated. Decomposition in flowing reactants (20% oxygen, (Figure 9), pure helium, (Figure 10), and in 5% propene, (Figure 11), all proceed by a reaction scheme denoted as Pathway 1 (effective heating rate of 1 K/min for XRD and 5 K/min for XAS). The XAS data for the decomposition in oxygen suggest that the X-ray amorphous phase, present after the second decomposition step, is similar to ATM. On the basis of the XAS data, the X-ray amorphous phase has to be divided into two categories, X-ray amorphous phase A, formed after the first decomposition step at ca. 340 K, and X-ray amorphous phase B, formed after the second decomposition step at ca. 470 K. The relatively low barrier for the transition between the two amorphous phases explains the continuous weight loss observed in the TG curves (Figure 4). The sequence of phases formed is (i) AHM, as the starting phase, (ii) X-ray amorphous phase A, at ca. 340 K, (iii) X-ray amorphous phase B (ATM) at 470 K, (iv) amorphous phase B is transformed into hexagonal MoO_3 at 520 K, and (v) final products, which differ according to the reducing potential of the gas phase [α-MoO_3 (O_2), Mo_4O_{11} (He), or MoO_2 (propene)].

Pathway 1:

$$\text{AHM} \xrightarrow{340\ \text{K}} \text{X-ray amorphous phase A} \xrightarrow{470\ \text{K}} \text{B(ATM)}$$
$$\xrightarrow{520\ \text{K}} \text{hex.}MoO_3 \xrightarrow{635\ \text{K}} \text{products}$$

The temperatures given for the decomposition steps should be considered only as reference points. They are a function of, not only the atmosphere, but also the heating rate and the gas flow rate.

The decomposition of AHM in 20% oxygen results in α-MoO_3, decomposition in helium results in α-MoO_3 and highly disordered Mo_4O_{11}, which recrystallizes with increasing temperature, and decomposition in 5% propene results in highly disordered Mo_4O_{11}, which is eventually reduced to MoO_2. The formation of highly dispersed Mo_4O_{11}, together with α-MoO_3 in the final step of the decomposition in helium is confirmed by the in situ XAS data (RDFs), which shows no change in the short-range structure with increasing temperature. The evolution of the corresponding edge-shift (Figure 13) reveals that the reduction takes place mainly during the decomposition of hexagonal MoO_3. A slight increase in the reduction with temperature is then observed, which is due to the mobility of lattice oxygen in this temperature region.[41] The changes observed by XRD after the decomposition of hexagonal MoO_3 are mainly due to recrystallization of Mo_4O_{11} with increasing temperature, and the formation of Mo_4O_{11} from MoO_3 and MoO_2.[29] The apparent oxidation during the decomposition of AHM at approximately 370 K (Figure 13) corresponds to the loss of NH_3 and H_2O during the formation of the amorphous phases (A+B), and thus oxidation of the remaining molybdenum oxide clusters. The Mo-*K* edge-shift observed during the decomposition in helium is representative for all decomposition conditions studied. However, under an oxidizing atmosphere (20% O_2 in helium), no reduction occurs during the decomposition of hexagonal MoO_3.

For the decomposition of AHM in a hydrogen containing atmosphere (Figure 15), Pathway 1 has to be modified. The XRD results indicate that the first decomposition step in hydrogen proceeds according to Pathway 1. The third decomposition step, however, yields MoO_3 with an unusual texture, instead of hexagonal MoO_3. With increasing temperature, α-MoO_3 is subsequently reduced to MoO_2.

The decomposition of AHM under static conditions follows a reaction scheme denoted as Pathway 2: (i) AHM, (ii) X-ray amorphous phase A, ca. 370 K, (iii) ATM is formed at ca. 500 K, followed by (iv) α-MoO_3 and hexagonal MoO_3, ca. 600 K, and (v) the decomposition of hexagonal MoO_3 to α-MoO_3 at 635 K. Since the influence of the heating rate may be more pronounced in a static atmosphere, larger differences were observed in the onset temperatures of the phase changes detected by in situ XRD and in situ XAS.

Pathway 2:

$$\text{AHM} \xrightarrow{370\ \text{K}} \text{X-ray amorphous phase A} \xrightarrow{500\ \text{K}} \text{ATM}$$
$$\xrightarrow{600\ \text{K}} \text{hex.} + \alpha\text{-}MoO_3 \qquad \xrightarrow{635\ \text{K}} \alpha\text{-}MoO_3$$

Structural Relationships Between Intermediates and Products

Following the given sequence of phases, the transformation from the cluster structure of AHM to the three-dimensional MoO_3 structure can be described as a polycondensation. In the structural sequences of the two monomers, hepta- and decamolybdate, and the one-dimensional oligomer, tetramolybdate, the structural unit of 6 Mo-O octahedra is preserved, as indicated in Figure 1. In the tetramolybdate, however, the octahedra in this 6 membered unit are tilted (Figure 1, C). Nevertheless, for structural rearrangement between these 3 phases, considerable mass transport has to be assumed. For the transition from the heptamolybdate to the decamolybdate, a complete rearrangement of the clusters is required. In the decamolybdate and in the tetramolybdate, the clusters, and thus the Mo-O octahedra, are all uniquely oriented, neglecting the slight tilt in the tetramolybdate. This unique orientation of the octahedra is retained in hexagonal and α-MoO_3. The density of the phases hepta-, deca-, and tetramolybdate are 2.46, 2.84, and 3.32 g/cm^3, respectively (not including NH_3 and H_2O molecules).

The water and ammonia ligands in AHM play an important role in the transformation process. In the AHM structure, all the NH_4^+ and H_2O ligands differ in their coordination to the molybdenum-oxygen clusters (some bridging,

some singly coordinated). However, since the loss of NH_4^+ is not stoichiometric from one phase to another and since the structural relationships between the phases are not obvious, it is difficult to deduce which of the ligand molecules is being removed during the individual transformation steps.

The polymers, α-MoO_3 and hexagonal MoO_3, possess no readily visible structural relationships with the monomers and the oligomer, and thus a reconstructive phase transformation has to be assumed. Hexagonal and α-MoO_3 can be described as two different arrangements of the same structural subunits. These subunits are chains of edge-sharing distorted Mo-O octahedra, which are orientated along the *c* axis in both structures, as indicated in Figure 1. In α-MoO_3, these chains are connected along the *a* axis via edge-sharing of the octahedra, forming a layer structure. In hexagonal MoO_3, the chains are arranged around a three-fold axis via edge-sharing of the octahedra, forming a three-dimensional network. The resulting density of α-MoO_3, 4.7 g/cm^3, is higher than that of hexagonal MoO_3, 3.97 g/cm^3, calculated for the structures (not including NH_3 and H_2O molecules).

The X-ray amorphous phase A in Pathway 1 and 2 could not be identified with the data available. Isothermal decomposition of AHM over extended periods of time (up to eight days) produced only amorphous phases or phase mixtures unsuitable for the identification of the X-ray amorphous phase A. With respect to the observation of ammonium decamolybdate in the literature, besides the role of the ammonia and water ligands in the kinetic inhibition of the formation of sufficiently crystalline ammonium decamolybdate, two structural features may hinder the formation of crystalline decamolybdate. The first is the necessary rearrangement of the clusters in a way that all Mo−O octahedra exhibit the same orientation, as described above. Secondly, in ammonium decamolybdate, two out of ten molybdenum atoms are coordinated by oxygen in a four-fold manner, rather than in a six-fold manner. The rearrangement of the Mo-O octahedra is observed in the formation of crystalline ATM, hexagonal MoO_3 and α-MoO_3. However, molybdenum is not coordinated by oxygen in a four-fold manner in any of the crystalline phases detected.

A Unifying Decomposition Scheme

A schematic representation of decomposition Pathways 1 and 2 is shown in Figure 17. In comparison with the results reported in the literature (Table 1), Pathway 2 is in good agreement with the in situ study 6. A few differences should be noted. They are the formation of ATM, together with the formation of hexagonal MoO_3 at approximately 445 K, and only hexagonal MoO_3 is detected without α-MoO_3during the third decomposition stage. These differences may be due to the limited 2θ range used for the XRD analysis in study 5. No ammonium decamolybdate is observed in study 5, which is in agreement with the study presented here. If an intermediate pathway between Pathway 1 and Pathway 2 is achieved (depending on the experimental conditions), only a small amount of crystalline ammonium decamolybdate may be formed. The agreement of the results of study 6 with those of this work indicates significant differences between the phases identified from in situ and ex situ experiments.

Considerable differences can be seen between this work and the other studies included in Table 1, which were primarily performed ex situ. With the exception of study 8, the other studies also identified ammonium tetramolybdate in the second decomposition stage, albeit in this study it is also found in an amorphous form under conditions which favors Pathway 1. Hexagonal MoO_3 formed during step three of Pathway 2 has only been reported in studies 5, 6, and 7. However, in study 5, hexagonal MoO_3 was prepared ex situ , from aqueous solution, in order to verify the results of the phase analysis of the third decomposition stage. Hexagonal MoO_3 is reported in the literature[35−38] to be metastable, which may be a reason that it is not detected in some ex situ studies. So far we have not succeeded in preparing hexagonal MoO_3 by decomposition of AHM under controlled conditions. Only mixtures of hexagonal and α-MoO_3 were obtained. Furthermore, the temperatures given for the formation of α-MoO_3 in studies 2, 3, 4, and 8 actu-

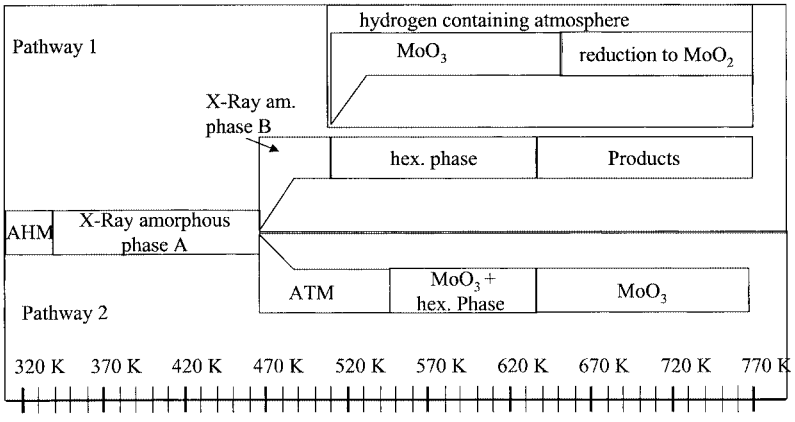

Figure 17. Schematic representation of the different pathways of the decomposition of AHM

ally correspond to step three in Pathway 2, where a mixture of hexagonal and α-MoO_3 is obtained.

With respect to the use of AHM as a catalyst precursor in the production of molybdenum oxide (MoO_{3-x}) based catalysts, the results show that it is possible, not only to control the reduction state but also the phase composition of the products. Apparently, this control can be most efficiently exerted at temperatures below ca. 520 K, where the molecular precursors persist with water as a spacer and ammonia as a counterion. In the temperature range from 610 K to 650 K, where molybdenum oxide catalysts exhibit the onset of catalytic activity, and hence are employed in the partial oxidation reactions of alkenes, the decomposition product obtained consists of partially reduced MoO_3 and mixtures of different oxides, rather than pure and defect-free MoO_3. In addition, this temperature range coincides with the onset of sufficient oxygen mobility in the molybdenum oxide lattice, a prerequisite for partial oxidation activity. This is in agreement with our previous results, that under partial oxidation reaction conditions, "MoO_3" corresponds to a partially reduced molybdenum oxide phase, probably with a considerable amount of shear-type defects in the regular structure. (For more detailed information see ref.[41] and references therein.)

This study demonstrates that control of the decomposition of AHM is possible. It is clear that the heating rate and reactant gas flow rate are coupled under the conditions investigated here. These parameters both function through their ability to affect the partial pressure of the gas phase decomposition products, which in turn control the decomposition path. This result indicates that it may be possible to direct the decomposition with a more complete control of the gas phase composition. Specifically, this control my be accomplished by purging with mixtures of product and/or reactant gases, with rates sufficient to minimize gas phase diffusion limitations and to allow only differential changes in the gas composition over the solid. This type of control could additionally be used to decouple the H_2O and NH_3 partial pressures, which are otherwise intrinsically coupled by the stoichiometry of the decomposition reactions.

Conclusion

The influence of the reactant atmosphere, and the heating rate and the gas flow rate on the decomposition of AHM has been shown. The results indicate that the decomposition scheme is sensitive to changes that affect the partial pressures of the gas phase decomposition products. In fact, differences in the gas phase product partial pressures, due perhaps to different flow rates, heating ramps, or experimental setups, are adequate to explain the differences in the results reported in the literature. The response of the system to changes in the gas phase decomposition product partial pressures is mainly important for the formation of hexagonal MoO_3, which depends on the preceding crystallization of ATM. Depending on the gas phase composition, two different Pathways can be distinguished:

Pathway 1 (low concentration of gaseous decomposition species at a given temperature)

(i) AHM; (ii) (≈ 335 K) X-ray amorphous phase A, (iii) (≈ 470 K) X-ray amorphous phase B (amorphous ATM), (iv) (≈ 520 K) hexagonal MoO_3; (v) (≈ 650 K) products (as a function of atmosphere, α-MoO_3, Mo_4O_{11}, or MoO_2).

Pathway 2 (high concentration of gaseous decomposition species at a given temperature)

(i) AHM, (ii) (≈ 350 K) X-ray amorphous phase A; (iii) (≈ 470 K) ATM.

(iv) (≈ 570 K) hexagonal MoO_3 + α-MoO_3; (v) (≈ 650 K) α-MoO_3.

Experimental Section

Ammonium Heptamolybdate Tetrahydrate: Ammonium heptamolybdate tetrahydrate, AHM, $(NH_4)_4Mo_7O_{24}\times 4\ H_2O$, was used as purchased (Aldrich, Analysis: total metallic impurities < 200 ppm). Phase purity and crystalline structure were verified by XRD and found to agree well with the simulated XRD powder patterns generated from single crystal data [ICSD 4153]. IR spectra of AHM were recorded with a FT-IR (Perkin−Elmer 2000), using the KBr disc technique. Chemical purity was confirmed by X-ray fluorescent analysis, which showed that there were no detectable impurities.

X-ray Diffraction: In situ XRD studies were performed with a Stoe STADI-P diffractometer (Ge secondary monochromator, Cu K_α radiation, Bragg−Brentano geometry), which is equipped with a Bühler HDK S1 high temperature cell (400 mL). Analysis of the gas phase was performed with a quadrupole mass spectrometer, QMS 200 (Pfeiffer), using a selective mass scan mode (≈ 12 s per scan). Measurements were performed in the temperature range from 300 K to 770 K, employing 2θ ranges of either 21.25−28.75° (short-range) or 5−45° (long-range). The shorter 2θ range was used to obtain more dynamic information, the longer 2θ range was sufficient for identification of the different phases. The short-range was selected in a 2θ region containing diffraction peaks of adequate intensities of all potential phases. With a heating rate of 5 K/min, diffractograms were recorded every 25 K for the long 2θ range, or every 15 K for the short 2θ range, resulting in effective heating rates of about 1 K/min or 0.1 K/min, respectively. The total gas flow rate was set to 100 mL/min. The concentrations of reactant gases in helium were 20% for oxygen, 5% for hydrogen, and 5% for propene. 30 mg of sample were suspended with acetone on the sample holder. A detailed description of the XRD set up can be found in Günter (2001).[28]

XRD studies of the ex situ samples were performed with a Stoe STADI-P diffractometer (Ge primary monochromator, Cu-K_α radiation, Debye−Scherrer geometry) equipped with a position sensitive detector.

Analysis of diffraction patterns was conducted using PowderCell for Windows, Version 2.3, and Stoe WinXPOW, Version 1.03. The ICDD (International center for diffraction data, former JC,PDS) database and the ICSD (Inorganic crystal structure database) were used for phase analysis.

X-ray Absorption Spectroscopy: In situ XAS measurements were performed in a flow reactor with a volume of ca. 4 mL, used in transmission geometry. Measurements were performed in a temperature range from 300 K to 770 K, with a heating rate of 5 K/·min.

The acquisition time was 4.5 minutes per spectrum, resulting in a temperature resolution of 22.5 K. Total flow rates of gases was set to 20 mL/min. Analysis of the gas phase was performed with a quadrupole mass spectrometer, QMS 200 (Pfeiffer), with a time resolution of ca. 12 s per scan using a selected mass scan mode. The AHM was mixed with boron-nitride (7 mg of AHM, 30 mg of BN) and pressed with a force of 1 ton into self-supporting pellets with a diameter of 5 mm. The resulting edge jump at the Mo-*K*-edge averages $\Delta\mu_x \approx 2$. For details of the experimental set up, see Ressler (2000).[29]

XAS measurements were performed at the Mo-*K* edge (19.999 keV) at the Hamburger Synchrotronstrahlungslabor, HASYLAB, beamline X1. The storage ring operated at 3.6 GeV with injection currents of 150 mA. A Si(311) double crystal monochromator was used.

Data analysis of the XAS spectra was performed using the software WinXAS 2.1.[30] The spectra were energy calibrated with respect to a molybdenum foil reference spectrum. Background subtraction and normalization were done using first order polynomials to fit the pre-edge and EXAFS region. Spectra were converted to k space using an E_0 defined as the second inflection point in the Mo-*K* edge. Atomic absorption, μ_0, fitting was performed using a cubic spline with 7 nodes and was optimized by minimization of peaks at low (< 1 Å) R value in the Fourier transformed $\chi(k)$.

Refinement of the local structure was performed in *R* space using the FEFF7 code[31] for calculation of amplitudes and phases for clusters with a radius of 6 Å around the absorber atom. The clusters were calculated from single crystal data of hexagonal and α-MoO_3 using the software Atoms.[32] All single scattering paths were considered, as well as multiple scattering paths with weights greater than 5% and a maximum of 4 legs. Fits were carried out in a range of ca. 0.4−3.9 Å, which resulted in 12 single scattering paths (SS) and 19 multiple-scattering paths (MS) for α-MoO_3 and hexagonal MoO_3. The number of free running parameters used during fitting was restricted to 19, well below the maximum of 28 allowed by the Nyquist theorem for the data range used. The free running parameters were (i) one Debye temperature for molybdenum and one for oxygen, (ii) one E_0 each for molybdenum and oxygen, (iii) - the distances of all SS paths, constrained to a maximum shift of ±0.1 Å, (iv) one third cumulant expansion factor for molybdenum and oxygen each and (v) the overall damping factor S_0.

TG/DTA: Weight loss measurements and differential thermal analysis (TG/DTA) were performed with a Seiko Instruments SSC/5200 (Pt-Rh 13% thermocouple). Measurements in 20% oxygen in helium and with a flow rate of 50 mL/min were carried out at heating rates of 0.5, 5, and 15 K/min. Three different flow rates 100 mL/min, 50 mL/min and no flow (static air), were examined with an atmosphere of 20% oxygen in helium and with a heating rate of 5 K/min. Additionally, a measurement in pure helium with a heating rate of 5 K/min and a flow rate of 50 mL/min was performed. Gas phase analyses were performed by using a Pfeiffer QMS 200 mass spectrometer.

Acknowledgments

We acknowledge the Hamburger Synchrotronstrahlungslabor HASYLAB for providing beam-time for this work. T. Ressler thanks the Deutsche Forschungsgemeinschaft "DFG" for financial support (Habilitationsstipendium). The authors are grateful to Prof. R. Schlögl for extended discussions and continuous support.

[1] A. J. Hegedüs, K. Sasvári, J. Neugebauer, *Z. Anorg. Allg. Chemie* **1957**, *293*, 56.
[2] M. Onchi, E. Ma, *J. Phys. Chem.* **1963**, *67*, 2240.
[3] E. Ma, *Bull. Chem. Soc. Jpn.* **1964**, *37(2)*, 171.
[4] E. Ma, *Bull. Chem. Soc. Jpn.* **1964**, *37(5)*, 648.
[5] M.-J. Schwing-Weill, *Bull. Soc. Chim. Fr.* **1967**, *10*, 3795.
[6] A. B. Kiss, P. Gadó, I. Asztalos, A. J. Hegedüs, *Acta Chim. Acad. Sci. Hung.* **1970**, *66(3)*, 235.
[7] A. Louisy, J. M. Dunoyer, *Bull. Soc. Chim. Fr.* **1970**, *67*, 1390.
[8] I. K. Bhatnagar, D. K. Chakrabarty, A. B. Biswas, *Indian J. Chem.* **1972**, *10*, 1025.
[9] Z. M. Hanafi, M. A. Khilla, M. H. Askar, *Thermochimica Acta* **1981**, *45*, 221.
[10] K. Isa, H. Ishimura, *Bull. Chem. Soc. Jpn.* **1981**, *54*, 3628.
[11] M. Topić, A. Moguš-Milanković, *Chroatica Chem. Acta* **1984**, *57(1)*, 75.
[12] I. B. Sharma, S. Batra, *J. Therm. Anal.* **1987**, *34*, 1273.
[13] W. J. Yong, *Thermochimica Acta* **1990**, *158*, 183.
[14] D. P. Shashkin, P. A. Shiryaev, M. Y. Kutyrev, O. V. Krylov, *Kin. Catal.* **1993**, *34(2)*, 302.
[15] S. A. Halawy, M. A. Mohamed, *J. Chem. Tech. Biotechnol.* **1993**, *58*, 237.
[16] A. A. Said, S. A. Halawy, *J. Therm. Anal.* **1994**, *41*, 1075.
[17] A. A. Said, *Thermochimica Acta* **1994**, *236*, 93.
[18] C. I. Cabello, I. L. Botto, H. J. Thomas, *Thermochimica Acta* **1994**, *232*, 183.
[19] M. Bi, H. Li, W.-P. Pan, W. G. Lloyd, B. H. Davis, *Thermochimica Acta* **1996**, *284*, 153.
[20] J.-C. Valmalette, R. Houriet, H. Hofmann, J.-R. Gavarri, *Eur. J. Solid State, Inorg. Chem.* **1997**, *34*, 317.
[21] Y. Zhoulan, L. Xinhai, C. Qiyuan, *Thermochimica Acta* **2000**, *352−353*, 107.
[22] C. Thomazeau, V. Martin, P. Afanasiev, *Appl. Cat. A* **2000**, *199*, 61.
[23] R. Murugan, H. Chang, *J. Chem. Soc., Dalton Trans.* **2001**, *20*, 3125.
[24] J.-L. Li, T. Inui, *Appl. Catal. A* **1996**, *137*, 105.
[25] J. Haber, E. Lalik, *Catalysis Today* **1997**, *30*, 119.
[26] R. K. Grasselli, *Catalysis Today* **1999**, *49*, 141.
[27] E. M. Gaigneaux, M. J. Genet, P. Ruiz, B. Delmon, *J. Phys. Chem. B* **2000**, *104*, 5724.
[28] M. M. Günter, T. Ressler, R. E. Jentoft, B. Bems, *J. Catal.* **2001**, *203*, 133.
[29] T. Ressler, R. E. Jentoft, J. Wienold, M. M. Günter, O. Timpe, *J. Phys. Chem. B* **2000**, *104*, 6360.
[30] T. Ressler, *J. Synchrotron Rad.* **1998**, *5*, 118.
[31] J. J. Rehr, C. H. Booth, F. Bridges, S. I. Zabinsky, *Phys. Rev. B* **1994**, *49*, 12347.
[32] B. Ravel, *J. Synchrotron Rad.* **2001**, *8*, 314.
[33] P. Kierkegaard, *Arkiv Kem.* **1964**, *23(21)*, 223.
[34] A. March, *Z. Kristallogr.* **1932**, *81*, 285.
[35] M. Maciejewski, E. Ingier-Stocka, W.-D. Emmerich, A. Baiker, *J. Thermal Anal.* **2000**, *60*, 735.
[36] J. L. Garin, J. M. Blanc, *J. Solid State Chem.* **1985**, *58*, 98.
[37] N. A. Caiger, S. Crouch-Baker, P. G. Dickens, G. S. James, *J. Solid State Chem.* **1987**, *67*, 369.
[38] J. Guo, P. Zavalij, M. S. Whittingham, *J. Solid State Chem.* **1995**, *117*, 323.
[39] I. L. Botto, C. I. Cabello, H. J. Thomas, *Mater. Chem. Phys.* **1997**, *47*, 37.
[40] I. L. Botto, A. C. Garcia, H. J. Thomas, *J. Phys. Chem. Solids* **1992**, *53(8)*, 1075.
[41] T. Ressler, J. Wienold, R. E. Jentoft, T. Neisius, *Journal of Catalysis*, **2002**, *210*, 67.

Received May 27, 2002
[I02275]